Realistic Modeling of Structural Steels with Yield Plateau Using Abaqus/Standard

Alper UCAK and Panos TSOPELAS

Department of Civil Engineering,
The Catholic University of America,
Washington, DC 20064

Abstract: *A new model for structural steel with capabilities to model yield plateau, as well as cyclic behavior is introduced. The model is incorporated into Abaqus/Standard through UMAT. Numerical results are presented for an application in earthquake engineering, where a steel bridge pier is excited with a quasi-static cyclic lateral load. Hysteresis loops and buckling patterns obtained from the computational model are compared with published experimental results.*

Keywords: *Constitutive Model, Plasticity, Experimental Verification, Earthquake Engineering, Low-cycle Fatigue, Buckling*

1. Introduction

In the current seismic design codes the so called performance-based design concept is promoted, where the structure is designed to achieve different levels of performance when subjected to different levels of seismic demand. This fairly new design concept requires methods to quantify the lateral displacement capacities of structural systems rather than the conventionally used lateral force capacity, which in turn requires reliable constitutive models that can correctly account for the non-linear material response under cyclic loading conditions.

Most structural steels, a commonly used construction material, show a distinct yield plateau followed by non-linear hardening region. The existence of this plateau region combined with the unique cyclic hardening and softening characteristics of the material constitutes a great difficulty from numerical modeling point of view. And despite the progress that has been made in computational mechanics, modeling structural steels with yield plateau is still a challenging task.

In this paper implementation of a constitutive model for structural steels with yield plateau into Abaqus/Standard via user element subroutines (UMAT) is presented. A brief description of the model, which is capable of capturing the response of the material for monotonic and cyclic loading conditions, is given. A practical application is presented to show the accuracy and capability of the developed model. Comparisons between the results obtained using the proposed model and the material models available in Abaqus/Standard are also presented.

2. Summary of Material Behavior

During monotonic uni-axial loading, after the initial homogenous elastic deformation, structural steels with yield plateau show a sharp yield point followed by the yield plateau. The plastic deformation along the yield plateau is caused by Luders bands (strain) propagation. During this process plastic deformation is in-homogenous along the gage. Once the Luders band cover the whole gage, the plastic deformation becomes homogenous and the material starts hardening. The hardening curve of the material is usually non-linear with respect to loading amplitude. From a macroscopic point of view the yield plateau region is treated as perfect plastic material without hardening, and the length of the plateau is quantified by the plastic strain value when hardening begins or ε_{sh}^{p}, as schematically depicted in Figure 1(a).

Material behavior under proportional cyclic loading is much more complex as compared with monotonic loading. Generally the monotonic hardening curve will not be representative of the cyclic characteristics of the material. However there exists one cyclic loading amplitude ($\varepsilon_{sh}^{p^*}$), for which the stabilized stress amplitude will coincide with the monotonic stress-strain curve. For fully reversed cyclic amplitudes grater than $\varepsilon_{sh}^{p^*}$, material will undergo cyclic hardening, while cyclic softening is observed for amplitudes smaller than $\varepsilon_{sh}^{p^*}$. This typical material response is schematically shown in Figure 1(b).

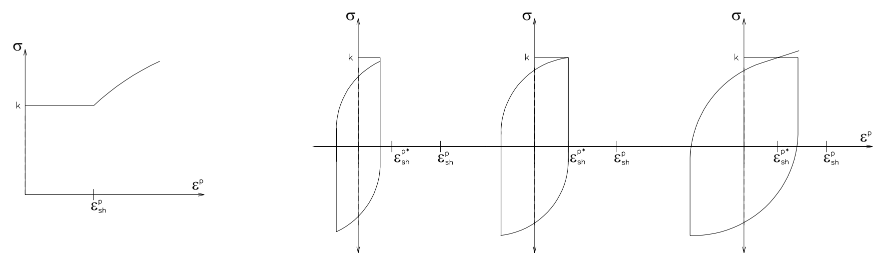

(a) (b)

Figure 1. Idealized material behavior; (a) for uni-axial loading; (b) for cyclic loading.

Experimentally determined back stress trajectories show that, along the yield plateau, the yield surface undergoes contraction with stabilization taking place approximately at the end of the plateau. After stabilization, the yield surface does not undergo any expansion; hence material hardening is caused by translation of the yield surface.

3. General Constitutive Equations

Additive decomposition of total strain ($\boldsymbol{\varepsilon}$) into elastic ($\boldsymbol{\varepsilon}^e$) and plastic ($\boldsymbol{\varepsilon}^p$) parts is assumed

$$\boldsymbol{\varepsilon} = \boldsymbol{\varepsilon}^e + \boldsymbol{\varepsilon}^p \tag{1}$$

where bold letters indicate second order tensors. The elastic strain components are related to the stress through Hook's law

$$\boldsymbol{\varepsilon}^e = \frac{1+\nu}{E}\boldsymbol{\sigma} - \frac{\nu}{E}\mathrm{tr}(\boldsymbol{\sigma})\mathbf{I} \tag{2}$$

where ν is the Poisson's ration, E is the Young's modulus of elasticity, $\boldsymbol{\sigma}$ is the stress tensor, $\mathbf{I}$ is the second order unit tensor and "tr" indicates the trace. The material is assumed to be initially isotropic. A von Mises criterion is assumed in the form

$$f = \left[\frac{3}{2}(\mathbf{s}-\mathbf{x}):(\mathbf{s}-\mathbf{x})\right]^{1/2} - \kappa \le 0 \tag{3}$$

$$\kappa = R + k \tag{4}$$

where the symbol ":" stands for contraction with respect to two indices; $\mathbf{s}$ is the stress deviator, $\mathbf{x}$ is the back stress, κ is the size of the yield surface, k is the initial size of the yield surface and R is the isotropic hardening/softening variable. An associative flow rule is assumed. During plastic flow the evolution law of the plastic strain and the accumulated plastic strain increment (dp) are expressed respectively as

$$d\boldsymbol{\varepsilon}^p = \lambda\frac{df}{d\boldsymbol{\sigma}} \tag{5}$$

$$dp = \left[\frac{2}{3}d\boldsymbol{\varepsilon}^p : d\boldsymbol{\varepsilon}^p\right]^{1/2} \tag{6}$$

where λ is the plastic multiplier to be determined using the consistency condition.

4. Description of the Constitutive Model

4.1 Memorization of the Plateau

Consistent with the observed material behavior, we assume existence of a plateau region and hardening region for both monotonic and cyclic loading conditions. Furthermore we assume that in the plateau region the maximum saturated stress can not exceed the initial yield stress of the virgin material designated with k. The transition from the plateau region to the hardening region depends on the maximum loading amplitude and the accumulated plastic strain. The loading amplitude is measured using a quadratic memory surface in the plastic strain space as proposed by Chaboche et al. (1979) and generalized by Ohno (1982):

$$g = \left[\frac{2}{3}\left(\boldsymbol{\varepsilon}^{p} - \boldsymbol{\xi}\right) : \left(\boldsymbol{\varepsilon}^{p} - \boldsymbol{\xi}\right)\right]^{1/2} - q \le 0 \tag{7}$$

where $\boldsymbol{\xi}$ and q are the center and radius of the memory surface. During plastic loading the memory surface changes location and size only if the plastic strain is located on the memory surface and the plastic strain increment is directed outwards of the memory surface. For this condition, the evolution rules for the radius and center of the memory surface are assumed to be

$$dq = \frac{1}{2} L_g (\mathbf{n} : \mathbf{n}^g) dp \tag{8}$$

$$d\boldsymbol{\xi} = \frac{1}{2} L_g d\boldsymbol{\varepsilon}^p \tag{9}$$

$$\left.\begin{array}{l} L_g = 1 \;\rightarrow\; g = 0 \text{ and } \mathbf{n} : \mathbf{n}^g \ge 0 \\[2ex] L_g = 0 \;\rightarrow\; g < 0 \text{ or } \mathbf{n} : \mathbf{n}^g < 0 \end{array}\right\} \tag{10}$$

where $\mathbf{n}$ and $\mathbf{n}^g$ are the normal to the yield surface and memory surface respectively. To distinguish between the plateau and hardening region the following condition is assumed:

$$q \le \varepsilon_{sh}^{p*} \text{ and } p \le \varepsilon_{sh}^{p} \rightarrow \text{plateau region} \tag{11}$$

$$q > \varepsilon_{sh}^{p*} \text{ and } p > \varepsilon_{sh}^{p} \rightarrow \text{hardening region} \tag{12}$$

4.2 The Plateau Behavior

To simulate the plateau behavior during monotonic loading, a bounding surface is incorporated into the deviatoric stress-space, which has the same shape and size as the yield surface of the virgin material. This bounding surface is not allowed to translate nor expand and/or shrink. During initial plastic loading, the yield surface shrinks and translates at the same time and is always in contact with the bounding surface at the loading point. The bounding surface is expressed as

$$\bar{f} = \left[\frac{3}{2}\mathbf{s} : \mathbf{s}\right]^{1/2} - k = 0 \tag{13}$$

The reduction of the elastic range is assumed to be in the form

$$R = R_\infty (1 - e^{-bp}) \tag{14}$$

where, R_∞ and b are material parameters. Equation (14) indicates an exponentially decaying function, which saturates to R_∞ $(-k<R_\infty<0)$. The material parameter b on the other hand dictates the rate of saturation. For consistency it has to be ensured that the yield surface is always in contact with the bounding surface at the loading point. Hence it is assumed, the outward normal of the yield surface and the bounding surface to be identical, leading to the following condition for the back stress

$$\mathbf{x} = \mathbf{s} - \frac{\kappa}{k}\mathbf{s} \tag{15}$$

The bounding surface which is used to simulate the plateau region during initial loading will vanish; (a) when equation (12) holds during monotonic loading or (b) if an unloading and reloading occurs while equation (11) is still holding. At this instance the backstress definition given in (15) will be changed as explained in the next section. Here we introduce a new internal parameter $\overline{\mathbf{x}}^{pl}$, which is the back stress value at the end of the yield plateau or the unlading back stress inside the plateau.

4.3 Unloading From the Plateau

Assume the material is pre-strained with plastic strain amplitude ε_0^p smaller than ε_{sh}^p and assume that the plateau condition given in equation (11) still holds. At this instance if the loading direction is changed, the bounding surface will vanish; i.e. Equations (13) and (15) will be deactivated and they will never be used again. Hereinafter the kinematic hardening variable $\mathbf{x}$ is assumed to consist for $M+N$ components

$$\mathbf{x} = \sum_{i=1}^{M}\mathbf{x}_i^{pl} + \sum_{j=1}^{N}\mathbf{x}_j^{h} \tag{16}$$

The first term on the right side of equation (16) is associated with the evolution of short-range kinematic hardening in the plateau region while the second term is associated with long-range kinematic hardening. In the plateau region the long range kinematic hardening variable $\mathbf{x}_j^h$ does not evolve, that is

$$\mathbf{x}_j^h = 0 \tag{17}$$

The evolution law for the short term back stress is expressed as (Armstrong and Frederick (1966)):

$$d\mathbf{x}_i^{pl} = \frac{2}{3}C_i d\varepsilon_p - \gamma(p)_i \mathbf{x}_i^{pl} dp \tag{18}$$

where, C_i is a material parameter, and the material dependent function $\gamma(p)_i$ is assumed in the form:

$$\gamma(p)_i = \gamma_i^{pl} \tag{19}$$

where γ_i^{pl} is a also material parameter. Some simple algebraic manipulations after analytical integration of (18) for a proportional tension-compression load path, leads to the absolute value of the saturated stress

$$\left|\sigma^{sat}\right| = \left[\left(\sum_{i=1}^{M}\frac{C_i}{\gamma_i}\right) + \kappa\right] \tag{20}$$

Since the condition given in equation (11) still holds, the material is not allowed to harden and the absolute value of the maximum saturated stress during cyclic loading must be the plateau stress or the initial yield stress of the virgin material, i.e.

$$\left|\sigma^{sat}\right| = k \tag{21}$$

Introducing equation (21) along with (4) into (20) and after some simple algebraic manipulations the following condition can be obtained

$$R = -\sum_{i=1}^{M}\frac{C_i}{\gamma_i} \tag{22}$$

With the right hand side of the above equation being constant, the condition given in equation (22) only makes physical sense if R is a constant. On the other hand the isotropic evolution law introduced in equation (14) indicates an exponentially decreasing function and R can only be equal to the constant R_∞ if the accumulated plastic strain value at the unloading is large enough so that the term e^{-bp} equation (14) vanishes At this point an assumption has to be made regarding the parameter b controlling the rate of saturation of the isotropic softening function. Unless it is ensured that the isotropic softening is completed inside the bounding surface before unloading occurs, it is impossible to create a consistent and thermodynamically stable model. Hence for consistency the unit less material parameter b that appears in equation (14) has to be large enough (say in the order of 10^5) to cause close to instantaneous saturation such that the isotropic function does not interfere with kinematic hardening function. With this crucial and necessary restriction, equation (22) is re-written as:

$$R_\infty = -\sum_{i=1}^{M}\frac{C^i}{\gamma^i} \tag{23}$$

Equation (23) will be used for material parameter determination purposes and will ensure that the hysteresis loops will return to the plateau stress. Finally an adjustment has to be made to the initial value of the backstress, $\mathbf{x}_i^o$, at the time of the fist unloading from the bounding surface. For consistency it must be assumed that

$$\sum_{i=1}^{M} \mathbf{x}_i^o = \overline{\mathbf{x}}^{pl} \tag{24}$$

which in turn leads to

$$\mathbf{x}_i^o = -\frac{1}{R_\infty}\frac{C_i}{\gamma_i^{pl}}\overline{\mathbf{x}}^{pl} \tag{25}$$

Numerical simulations show that superposition of two kinematic hardening functions (or M=2), produces acceptable hysteresis loops, without creating storage problems during finite element applications.

4.4 Hardening Behavior

At the instance, when equation (12) is satisfied, the existing memory of the material is erased and reset with the following initial conditions:

$$\boldsymbol{\xi} = \overline{\boldsymbol{\varepsilon}}^{p},\ q = 0 \tag{26}$$

where $\overline{\boldsymbol{\varepsilon}}^{p}$ is the plastic strain value at which equation (12) is satisfied. Also the evolution rules given in equations (8) and (9) are re-defined to allow for progressive memory effects as:

$$dq = c_g L_g (\mathbf{n} : \mathbf{n}^g) dp \tag{27}$$

$$d\boldsymbol{\xi} = (1 - c_g) L_g d\boldsymbol{\varepsilon}^p \tag{28}$$

where c_g is a scalar material parameter ($0<c_g\leq 0.5$). Note that for the particular value of $c_g=0.5$ equations (27) and (28) become identical to (8) and (9), and memorization is instantaneous. The evolution law for the long term kinematic hardening variable is assumed to be in the form:

$$d\mathbf{x}_j^h = \frac{2}{3} C_j d\varepsilon_p - \gamma_j \mathbf{x}_j^h dp \tag{29}$$

Cyclic hardening is incorporated to the model trough a modification to one of the material dependent functions given in equation (18), such that

$$\gamma(p)_1 = \gamma_1^\infty - (\gamma_1^\infty - \gamma_1^{pl}) e^{-wp} \tag{30}$$

where γ_1^∞ and w are material parameters. To account for material memory effects, the following restriction is imposed to equation (30):

$$d\gamma(p)_1 = w(\gamma_1^{\infty} - \gamma_1^{pl})dpL_g \tag{31}$$

The proposed material model is implemented to Abaqus/Standard using the user material subroutine (UMAT). The integration algorithm implemented, consists of a closest point projection scheme similar to one described in Ortiz and Simo (1986).

5. Numerical Simulations

Fukumoto (2004) tested large scale, cantilever thin walled steel columns, with stiffened box cross-sections, under constant axial and cyclic horizontal loading. To verify the constitutive model developed, one of the tested columns, TPRC 9-9, was and analyzed with the general purpose finite element code Abaqus/Standard.

Schematic presentation of the experimental setup used by Fukumoto (2004) and the corresponding FE model are depicted in Figure 2(a) and (b) respectively. As shown in Figure 2(a), the specimen used was a *2289 mm* long stiffened box section, consisting of *450x9 mm* flange and web plates and two equally spaced *60x6 mm* vertical stiffeners. Furthermore the specimen was divided into five panels with four horizontal *6 mm* thick horizontal diaphragms. During the experiments the axial load was kept constant at 15% of the axial yield load or $P=0.15\cdot A\cdot k$, where A is the cross-sectional area of the specimen and k is the material yield stress. The steel grade used was SS400 (Japanese origin, A36 equivalent) mild steel, with yield stress (k) equal to 266 MPa. The lateral load path consisted of a displacement controlled cyclic motion of increasing amplitude, as multiples of the yield displacement of the column d_o, i.e.$\pm d_o$, $\pm 2d_o$, $\pm 3d_o$, …, during which the horizontal load (H) is monitored at the loading point. The yield displacement of the column (d_o) can be calculated as

$$d_o = \frac{H_o h^3}{3EI} \tag{32}$$

$$H_o = \left(k - \frac{P}{A}\right)\frac{Z}{h} \tag{33}$$

where h is the column height, I is the moment of inertia, Z is the section modulus and H_o is the yield load.

The FE model used is depicted in Figure 2(b). It consists of SR4 shell elements, B33 beam elements and RB2D2 rigid links, all of which are available in Abaqus/Standard element library. Using symmetric boundary conditions only half of the column is discretized in the analyses. At the base, fixed boundary conditions are applied. Preliminary analyses conducted have shown that in box section stiffened cantilever steel columns, localized deformation is concentrated in the lowest section of the column, close to its base, which is in agreement with the experimentally established deformation patterns. Given this typical behavior only the lover half of the column is discretized with SR4 shell elements (including flange, web, vertical stiffeners and diaphragms) while the upper part is modeled using B33 beam elements. The beam elements are connected to shell elements using rigid links. The mesh density of the analyzed circular columns is determined using a trial and error approach.

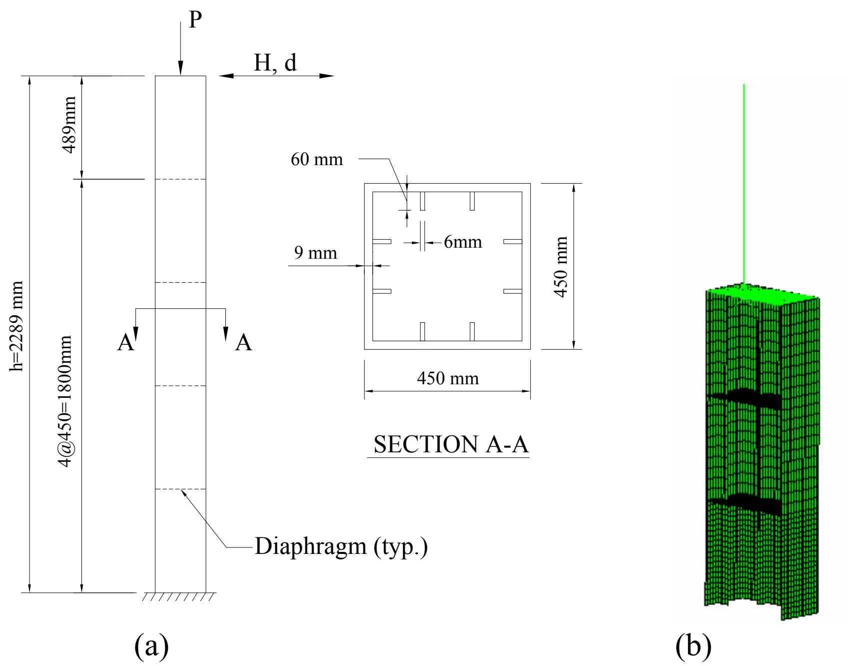

Figure 2. (a) Schematic presentation of the test setup used by Fukumoto (2004) (1996); (b) FE model utilized in this study

The material properties of the proposed model are calibrated using generic material properties reported by Fukumoto (2004). Resulting material parameters are given in Table 1. The simulated material responses under uni-axial and proportional cyclic tension-compression loading conditions are shown in Figure 3(a) and 3(b) respectively. To facilitate comparison between the proposed constitutive model and the ones already available in Abaqus/Standard material library, two additional solutions are presented, in which the material non-linearity is modeled with non-linear kinematic hardening rule. For the first solution, designated with "NLKH-M", cyclic hardening of the material is omitted and the material parameters are calibrated to fit the uni-axial stress curve of the material, given in Figure 3(a). For the second solution, "NLKH-C", material parameters are chosen such that in a fully reversed cyclic test, the stabilized stress amplitudes for plastic strain amplitudes between 0.5-3%, are the same as the once produced by the proposed model. The final material properties for the "NLKH-M" and "NLKH-C" models are listed in Table 2. The resulting uni-axial stress strain curves and the stabilized stress amplitudes as a function of cyclic strain amplitudes are superimposed into Figure 3(a) and 3(b) respectively.

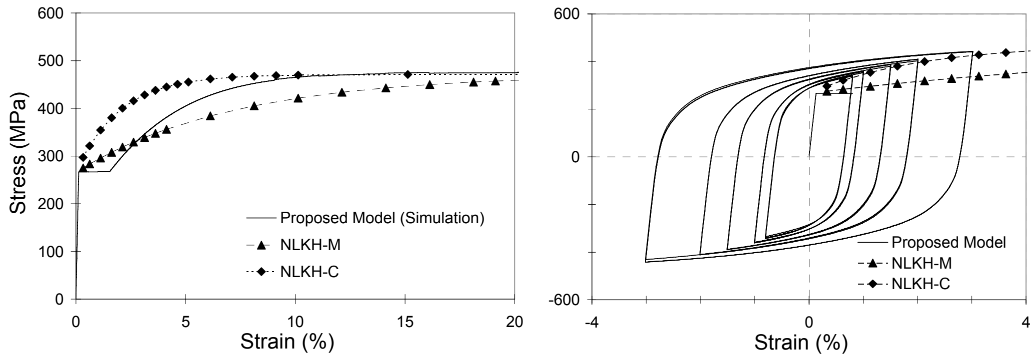

(a) (b)

Figure 3. Idealized material behavior; (a) for uni-axial loading; (b) for cyclic loading.

Table 1. Material parameters used for the proposed constitutive model

Parameter	E (GPa)	ν -	k (MPa)	ε_{sh}^{p} (%)	ε_{sh}^{p*} (%)	R_∞ (MPa)	b -	C_1 (GPa)	γ_1^{pl} -	γ_1^{∞} -	w -
Value	206	0.30	266	1.50	0.40	$-0.4 \cdot k$	10^5	26.60	1000	340	45

Parameter	C_2 (GPa)	γ_2^{pl} -	C_3 (GPa)	γ_3 -
Value	399.00	5000	5.15	33

Table 2. Material parameters used for the non-linear kinematic hardening rule

	E (GPa)	ν -	k (MPa)	C (GPa)	γ –
NLKH-M	206	0.3	266	2.66	14
NLKH-C	206	0.3	266	10.25	50

Figure 4 compares the hysteretic loops obtained from the FEM analyses with the ones reported by Fukumoto (2004) for the stiffened box column TPRC 9-9. In Figure 4, the normalized horizontal displacement at the loading point is plotted in the abscissa and the corresponding normalized shear force (horizontal force) is plotted in the ordinate. Here it must be noted, since the test results were not available to the authors, the experimental force-deformation curves, which are reported here in, are obtained by digitizing the figures in the original publication by Fukumoto (2004).

Comparison of the hysteretic curves presented in Figure 4 shows that the numerical results are in close agreement with the experimental ones. The FE model predicts shape of the hysteresis curves, the buckling load, the maximum deformation capacity, as well as the stiffness deterioration and the strength degradation accurately. And in spite of the minor errors, part of which is introduced to the analyses due to lack of cyclic coupon data, the results produced by the proposed model are more than satisfactory.

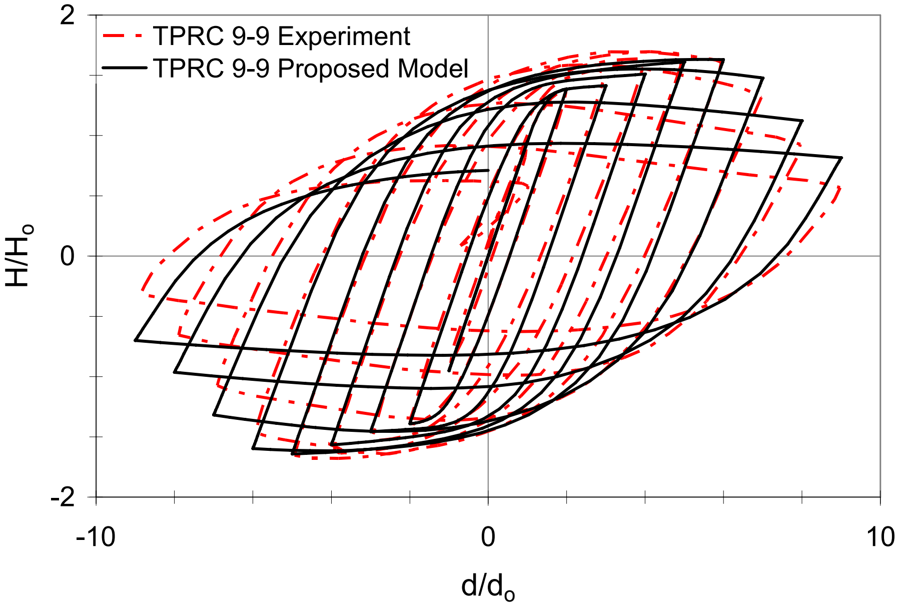

Figure 4. Experimental vs. FE analysis results for stiffened box column TPRC 9-9 (experimental data after Fukumoto 2004)

Figure 5 shows the final deformed shape obtained from FE analyses along with the experimentally observed deformation pattern (Fukumoto 2004). Inspection of Figure 5 reveals that the analytical model successfully captures the global plate buckling mode observed in the experiments, that has a half sine-wave shape, inward in flanges and outward in web.

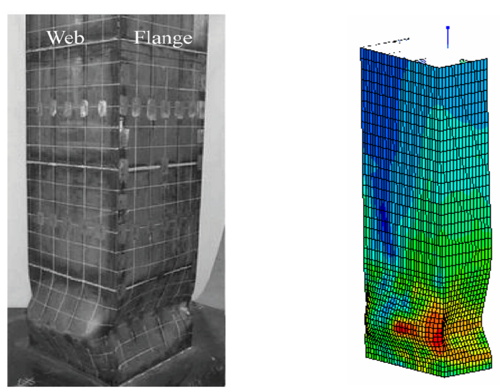

Figure 5. Comparison of the final buckled shape analytically obtained using the proposed model and experimentally observed (experimental data from Fukumoto 2004).

Figure 6 compares the hysteresis loops obtained from the analyses designated as "NLKH-M", and "NLKH-C" with the experimental data. As clearly visible from these graphs, when the cyclic properties of the material are omitted (model "NLKH-M") the ultimate strength of the specimen is underestimated. The "NLKH-C" model on the other hand, which accounts to certain extend for the stabilized material behavior, overestimates both the strength and deformation capacity of the column. Although both the performance of the "NLKH-M" and "NLKH-C" models are somewhat disappointing, the solutions produced by these models are still acceptable, especially given their simplicity. However, in cases where the non-linear kinematic hardening rule is to be used to model material non-linearities, it is recommended that multiple analyses should be carried out with material models calibrated using monotonic and cyclic coupon data, since the real solution seems to lie somewhere between these two cases.

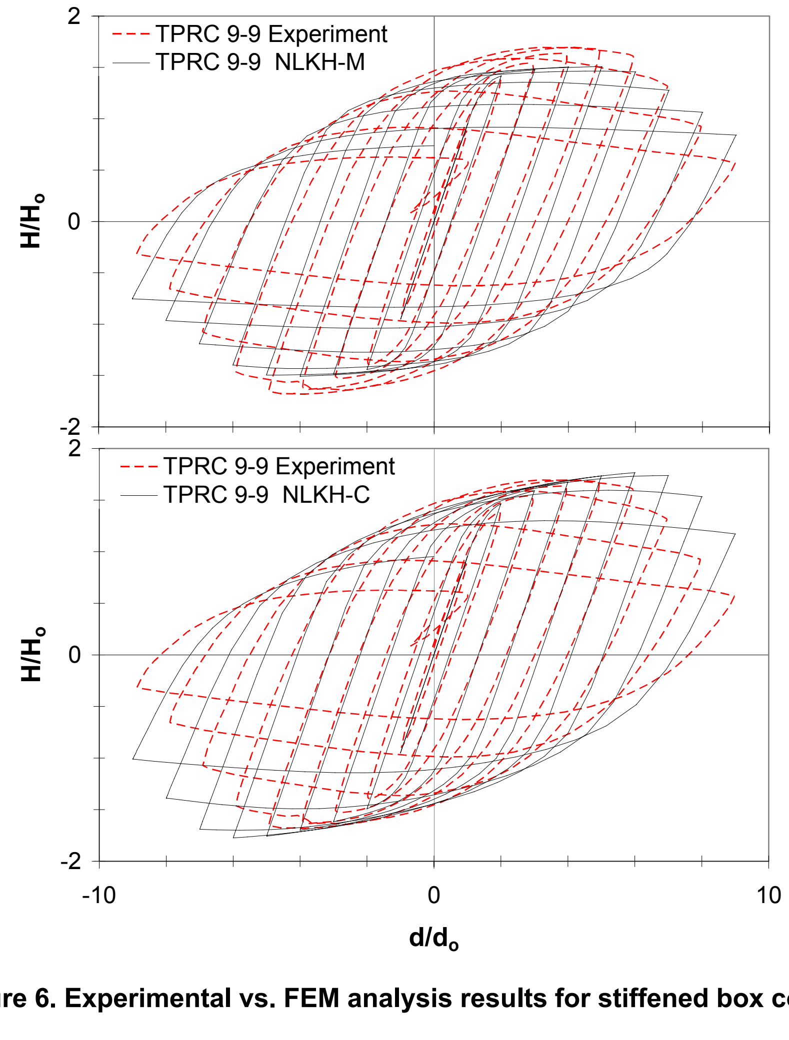

Figure 6. Experimental vs. FEM analysis results for stiffened box column

6. Conclusions

A new constitutive model is proposed for structural steels with yield plateau. The model can correctly capture both the yield plateau and the progressive cyclic hardening commonly observed in structural steels. The proposed model is validated against published experimental data. It is shown that the constitutive model can accurately capture the experimental force-deformation loops of a thin walled circular steel pier under constant axial load and horizontal cyclic motion of progressively increasing nature.

7. References

1. Armstrong, P.J. and Frederick, C.O., “A Mathematical Presentation of the Multiaxial Bauschinger Effect,” CEGB Report No. RD/B/N731, 1966
2. Chaboche, J.L., Dang-Van, K., Cordier, G., “Modelization of Strain Memory Effect on the Cyclic Hardening of 316 Stainless Steel,” Transactions of the 5th International Conference on Structural Mechanics Reactor Technology, vol. L, paper no. 11/3, 1979
3. Fukumoto, Y., “Cyclic Performance Assessment of Stiffened Box Columns with Thickness Tapered Plates” Proceedings of the 2004 Annual Stability Conference, SSRC, pp.1-18, 2004.
4. Ohno, N., “A Constitutive Model of Cyclic Plasticity with a Nonhardening Strain Region,” Journal of Applied Mechanics, ASME, vol.104, pp.721-727, 1982.
5. Ortiz, M. and Simo, J.C., “A Return Mapping Algorithm for Plane Stress Elastoplasticity,” International Journal for Numerical Methods in Engineering, vol. 22, pp.649-670, 1986.